Author Manuscript

Author Manuscript

Author Manuscript

Author Manuscript

HHS Public Access

Author manuscript

Biol Psychiatry. Author manuscript; available in PMC 2021 October 15.

Published in final edited form as:

Biol Psychiatry. 2020 October 15; 88(8): 638–648. doi:10.1016/j.biopsych.2020.05.009.

Transcriptional Profiling of Primate Central Nucleus of the Amygdala Neurons to Understand the Molecular Underpinnings of Early Life Anxious Temperament

Rothem Kovner[1,2,3,*], **Tade Souaiaia**[4], **Andrew S. Fox**[5,6], **Delores A. French**[1,3], **Cooper. E. Goss**[1], **Patrick H. Roseboom**[1,2,3], **Jonathan A. Oler**[1,3], **Marissa K. Riedel**[1,3], **Eva M. Fekete**[1,3], **Julie L. Fudge**[7,8], **James A. Knowles**[4], **Ned H. Kalin**[1,2,3]

[1]Department of Psychiatry, University of Wisconsin, Madison, WI, USA

[2]Neuroscience Training Program, University of Wisconsin, Madison, WI, USA

[3]HealthEmotions Research Institute, University of Wisconsin, Madison, WI, USA

[4]Department of Cell Biology, State University of New York Downstate Medical Center, Brooklyn, NY

[5]Department of Psychology, University of California, Davis, CA, USA

[6]California National Primate Research Center, University of California, Davis, CA, USA

[7]Department of Psychiatry, University of Rochester Medical Center, NY, United States

[8]Department of Neuroscience/Del Monte Institute for Brain Research, University of Rochester Medical Center, NY, United States

Abstract

Background: Children exhibiting extreme anxious temperament (AT) are at an increased risk to develop anxiety and depression. Our previous mechanistic and neuroimaging work in young

[*]Corresponding author: Rothem Kovner, kovnerrothem@gmail.com.

Contributions

RK, ASF, JAO, PHR and NHK conceptualized the study. NHK and ASF oversaw the study. RK, MKR, and EMF collected behavioral data. RK and DAF developed the rapid staining laser-capture microdissection (LCM) microscopy method and collected the RNA data. DAF performed RNA extractions. JAK and his group performed RNA-Seq. TS aligned the RNA-Seq data. RK and TS analyzed the RNA-Seq data. RK, MKR, and PHR collected tissue and PHR assessed cortisol. JLF, NHK, and RK conceptualized the stereology study. RK and CEG collected and analyzed the stereology data. JLF performed retrograde tracer surgeries and collected injected tissue. RK performed triple labeling of tracing experiments and microscopic analysis. RK and NHK wrote the paper.

Publisher's Disclaimer: This is a PDF file of an unedited manuscript that has been accepted for publication. As a service to our customers we are providing this early version of the manuscript. The manuscript will undergo copyediting, typesetting, and review of the resulting proof before it is published in its final form. Please note that during the production process errors may be discovered which could affect the content, and all legal disclaimers that apply to the journal pertain.

Financial Disclosures

NHK has received honoraria from CME Outfitters, Elsevier, and the Pritzker Consortium; has served on scientific advisory boards for Actify Neurotherapies and Neuronetics; currently serves as an advisor to the Pritzker Neuroscience Consortium and consultant to Corcept Therapeutics; has served as co-editor of Psychoneuroendocrinology and currently serves as Editor-in-Chief of The American Journal of Psychiatry; and has patents on promoter sequences for corticotropin-releasing factor CRF2α and a method of identifying agents that alter the activity of the promoter sequences (7,071,323; 7,531,356), promoter sequences for urocortin II and the use thereof (7,087,385), and promoter sequences for corticotropin-releasing factor binding protein and the use thereof (7,122,650). All other authors report no biomedical financial interests or potential conflicts of interest.

Author Manuscript Author Manuscript Author Manuscript Author Manuscript

rhesus monkeys links the central nucleus of the amygdala (Ce) to AT and its underlying neural circuit.

Methods: Here, we used laser capture microscopy and RNA sequencing in 47 young rhesus monkeys to investigate AT's molecular underpinnings by focusing on lateral Ce (CeL) neurons. RNA sequencing identified numerous AT-related CeL transcripts and we used immunofluorescence (n=3) and tract-tracing (n=2) methods in a different sample of monkeys to examine the expression, distribution, and projection pattern of neurons expressing one of these transcripts.

Results: We found 555 AT-related transcripts, of which 14 were confirmed with high statistical confidence (FDR<0.1), including protein kinase C type-delta (PKCδ), a CeL microcircuit cell marker implicated in rodent threat processing. We characterized PKCδ neurons in the rhesus CeL, compared its distribution to that of the mouse, and demonstrated that a subset of these neurons project to the laterodorsal bed nucleus of the stria terminalis (BSTLd).

Conclusions: These findings demonstrate that CeL PKCδ is associated with primate anxiety, provides evidence of a CeL to BSTLd circuit that may be relevant to understanding human anxiety, and points to specific molecules within this circuit that could serve as potential treatment targets for anxiety disorders.

Keywords

fear; anxiety; stress; central nucleus of the amygdala; bed nucleus of the stria terminalis; microcircuitry; protein kinase C type delta; PKCδ; somatostatin; retrograde tracing

Introduction

Depending on its intensity and the context in which it is expressed, anxiety can be adaptive or maladaptive. Across a population anxiety is characterized by individual differences, and when extreme is disabling. Research has identified heritable and non-heritable factors underlying the development of anxiety disorders (1–4), and in childhood these can manifest as the trait-like disposition, anxious temperament (AT). Like anxiety, AT is dimensional and is characterized by individual differences in inhibitory responses to novel and social situations (5–8) as well as threat-related pituitary-adrenal activation (5, 9). Because AT reflects a combination of behavioral and physiological responses to stress, this construct reflects the interplay between emotions, behavior and physiology that is emblematic of anxiety responses. When extreme and stable over time, childhood AT increases the risk for the development of anxiety disorders, depression, and co-morbid substance use disorder later in life (6, 7, 10–12).

To understand the mechanisms underlying AT, we developed a young rhesus monkey model of individual differences in the expression of dispositional anxiety that is analogous to the phenotype exhibited by at-risk children (13, 14). Rhesus monkeys are ideally suited for studies of human psychopathology due to their recent evolutionary divergence from humans, which is reflected in similarities in brain structure, and emotional and physiological responding (14). Our approach is to understand individual differences in the AT phenotype in relation to individual differences in its underlying neural and molecular substrates (4, 13,

Author Manuscript Author Manuscript Author Manuscript Author Manuscript

15). Using a large multigenerational pedigree, we demonstrated that AT is ~30% heritable, consistent with previous human studies (4, 16).

Numerous studies point to the importance of the extended amygdala in mediating adaptive responses to threat as well as in stress-related psychopathology (13, 17, 18). Components of the extended amygdala include the central nucleus of the amygdala (Ce) and the bed nucleus of the stria terminalis (BST; (19). The Ce, primarily composed of GABAergic neurons, coordinates information flow out of the amygdala (20–24). The Ce sends strong projections to the BST, a region also involved in threat-responding (25–27). We previously demonstrated that individual differences in Ce and BST metabolism relate to trait-like individual differences in AT (5), that brain metabolism in these regions is heritable, and that BST, but not Ce, metabolism is co-heritable with AT (4). We also demonstrated that neurotoxic lesions of the Ce reduce AT, directly implicating the Ce as a core mechanistic component of the AT circuit (4, 28, 29).

It is important to emphasize that the Ce is not uniform and can be divided into at least 2 subnuclei including the lateral Ce (CeL) and medial Ce (CeM; (30, 31). The CeM coordinates the output of the amygdala via its projections to multiple downstream effector sites (24). The CeL modulates the CeM, helping to orchestrate the different behavioral and physiological responses mediated by the CeM's targets (21, 32). The entire Ce projects to the BST to further coordinate threat-related responding, where the CeL's projections are largely restricted to the laterodorsal BST (BSTLd; (25, 33–35). In addition to other basal forebrain areas, the CeL, CeM, and the BSTLd have been conceptualized as the central extended amygdala (19). Rodent studies have traced microcircuits within the extended amygdala that are comprised of GABAergic neuronal subtypes acting to mediate anxiety and fear responses (23, 32–35). However, these microcircuits have not yet been characterized in primates.

In this study, we characterized individual differences in gene expression in laser microdissected primate CeL neurons in relation to AT and its components by performing RNA sequencing (RNA-Seq). We focused on CeL neurons because of its mechanistic role in mediating primate AT and because of rodent data demonstrating the CeL's role integrating information and acting as an interface between the basolateral amygdala and the CeM/BSTLd (23, 26, 36, 37). Rodent studies have also highlighted subpopulations of GABAergic CeL neurons, for example protein kinase C type delta (gene: *PRKCD,* protein: PKCδ) and somatostatin (gene: *SST,* protein: SST), that have critical roles in modulating fear- and anxiety-related extended amygdala function (20, 32, 38, 39). Here, in addition to our discovery-based approach, we more specifically focused on genes known to distinguish CeL neuronal subtypes. Because the RNA-Seq data revealed relations between *PRKCD* expression and AT, as an initial step to understand extended amygdala microcircuitry in the primate, we characterized the distribution and projection pattern of PKCδ neurons within the extended amygdala. This approach informs the translational value of rodent anxiety models to primates, and because of the relevance of the rhesus AT model to humans, the findings have the potential to uncover novel molecular targets for the treatment of anxiety disorders and other stress-related psychopathology.

Author Manuscript Author Manuscript Author Manuscript Author Manuscript

Methods and Materials

Complete methods are found in Supplement 1.

Anxious Temperament Phenotyping

AT is a composite score reflecting threat-related behavioral and cortisol changes elicited by exposure to the no eye contact condition of the human intruder paradigm (5). Freezing duration and coo vocalization reductions along with plasma cortisol levels were used to compute each individual's AT (Supplement 1).

Animals

Forty-seven monkeys (*Macaca mulatta*; average age=2.27 years, std=0.46, 24 males and 23 female) were used for RNA-Seq. To understand the AT levels in these 47 animals in relation to a larger population from which they came, we performed an analysis with data from animals that were phenotyped in our laboratory over the last 12 years (n=721, average age=1.9 years, std=0.74, 386 males and 335 females, Supplement 1, Figure S1B). C57BL/6J and KO;B6;129X1-*Prkcd*^{tm1Msg}/J mice (The Jackson Laboratory; Bar Harbor, ME) were group housed for at least 7 days before experimentation (12-hour light/dark cycle; *ad libitum* access to food and water). When 21 days old, mice were perfused (40), and tissue was stored for immunohistochemical studies. Animal housing and experimental procedures were in accordance with institutional guidelines and were approved by the Committee on the Ethics of Animal Research of the University of Wisconsin.

Laser Capture Microdissection

All monkeys were euthanized under deep anesthesia, 4 days after AT phenotyping, with the guidance of veterinary staff using pentobarbital, consistent with the recommendations of the Panel on Euthanasia of the American Veterinary Medical Association. Fresh frozen tissue was collected, cut into slabs, flash frozen in 2-methylbutane, and stored at −80°C as previously described (41). 14μm sections from the slab containing the amygdala were obtained on a cryostat at −20°C. Sections throughout the CeL's anterior-posterior (A-P) extent were mounted on Leica PEN 2.0μm membrane laser capture microdissection (LCM) slides (11532918, Leica, Wetzlar, Germany). Adjacent sections were stained with acetylcholinesterase (AChE) to localize the Ce (Figure S2B). LCM sections were rapidly stained for NeuN (Supplement 1). CeL neurons were dissected with a Leica LMD6500 laser capture microscope. For each animal, 500–600 neurons were sampled from 6–8 slides (every 0.25mm). After dissection, each LCM slide image was overlaid with its adjacent AChE slide image in Adobe Illustrator CC 2014 to confirm that cells were dissected from the CeL. Tubes containing a minimum of 80% of neurons captured from the CeL were used and the percent of CeL neurons in each of these tubes was used to calculate a "CeL neuronal accuracy" score (Supplement 1). Within an animal, tubes were pooled for RNA extraction using Qiagen RNeasy Plus micro kit (74034, Qiagen, Hilden, Germany).

RNA Sequencing

RNA was sequenced at USC by Dr. Knowles. Samples were processed with NuGen RNA-Seq V2 kit (7102-32, NuGen, San Carlos, CA) for cDNA synthesis and NuGEN Ovation

Author Manuscript Author Manuscript Author Manuscript Author Manuscript

Rapid library kit (0319, 0320, NuGen) for library preparation. The Illumina Hiseq 2500 with regular rapid sequencing prep kit was used. Reads were single end and targeted to be 100bp in length. A mean of 949710 mapped reads was found across animals. Reads were mapped to MacaM 7.8 (42). Mapping was performed using Sequence Alignment for Gene Expression (https://github.com/tadesouaiaia/sage) written in python 2.7.

RNA Sequencing Analysis and Model Evaluation

Genes with 1 read in at least 20% of the animals were used for quantile normalization. Data was log2 transformed and fully annotated genes where at least 50% of the samples expressed more than 1 mapped read were used in ordinary least squares (OLS) regression. We built statistical models that assessed the association between gene expression and the predictor of interest. AT, freezing, cooing, and cortisol measured closest to time of death were used as predictors. The statistical model was built within a framework designed to maximize power to detect predictor-related associations while also reducing false positives discovered with permutation analysis. We focused on models which described the largest fraction of the variance (R^2) across the transcriptome without overfitting.

Variables were tested in relation to transcriptome-wide gene expression to identify potential covariates and tested for collinearity (Figure S3A). Two measures (CeL neuron accuracy, age at necropsy) were selected as they were not multicollinear and had the greatest number of positive genes relative to false positives in a simulation (Supplement 1; Table S1). Using CeL neuron accuracy and age at necropsy as covariates separately and together, we tested models to establish whether they could detect predictor-related gene expression relationships above chance. Sex was not included as it did not perform better than a pseuodo variable and did not improve upon the variance accounted for by a model without sex (Table S2). We chose the models using both neuron accuracy and age at necropsy because they had the lowest BIC, accounted for the greatest percentage of the variance, and had the fewest false positives in a simulated model. In the models using AT, freezing, cooing, and cortisol as predictors, the predictor was shuffled and correlated with gene expression. Chance distributions were constructed with 10,000 simulations for each predictor (Figure 1A) to assess the signal strength relative to noise. The final model was used to determine differentially expressed (DE) genes associated with each predictor. OLS regression and permutation testing (Supplement 1) was performed in python 2.7. Another DE analysis was performed using DESeq2 (43). Gene ontologies were investigated using Panther (44).

Results

AT as a predictor of the CeL neuronal transcriptome compared to its individual components

LCM was combined with RNA-Seq to identify CeL neuronal gene expression (Figure S2A; Figure S3B–C) associated with individual differences in AT and its components (Figure 1A). Because our previous work demonstrated that AT accounts for greater variance in CeL metabolism than its components (45), we explored the hypothesis that AT would better predict gene expression than each of its components. After demonstrating that the AT scores of the 47 animals used here were representative of a larger population (n=721; Figure S1B;

Author Manuscript Author Manuscript Author Manuscript Author Manuscript

Supplement Results), multiple regression was used to investigate the relation between gene expression and each predictor (AT, freezing, cooing, cortisol). We performed a permutation analysis where 10,000 shuffles were performed for each predictor and correlated with transcript expression to construct simulated null distributions of the number of genes associated with each predictor at chance (Figure 1A). Results demonstrated that AT performed significantly better than chance (empirical p=0.04, Figure 1B) whereas AT's individual components did not. Furthermore, the number of genes that were above chance predicted by AT was significantly greater than the number predicted by AT's components (Figure 1C). 555 genes were significantly associated with AT, 383 genes were significantly associated with at least one of AT's components, and 172 genes were significantly and selectively correlated with AT (Figure 1D; Supplement Results; Figure S5). A similar pattern was observed after performing a weighted gene co-expression network analysis (Supplement Results; Figure S6).

Specific CeL neuronal transcripts associated with AT

Two different approaches were used to identify AT-associated genes. Using DESeq2 (43), which utilizes a negative binomial model, we identified 716 AT-related genes ($p<0.05$; Table S2) constituting 11% of the total genes tested, with 42 genes passing multiple comparison correction (FDR<0.1). In addition, we also utilized an ordinary least squares (OLS) approach with log transformed data which identified 555 AT-related transcripts, comprising 6% of the total genes tested ($p<0.05$; Table S2). To account for multiple testing, we performed a non-parametric permutation test on the correlation between AT and gene expression, identifying 20 genes (FDR<0.1; Supplement 1). The conjunction of the FDR corrected genes between the DESeq2 and OLS analyses yielded 14 gene (Table 1; Table S2). GO enrichment analyses on the genes identified with each approach (Figure 2A) demonstrated several biological processes (Table S3) in common including neuron projection (GO:0043005), cell projection regulation (GO:0031344), and G-protein receptor activity (GO:0031344; Figure 2B; Table S3).

Among the 14 transcripts that passed FDR correction with both methods, several were related to epigenetic mechanisms such as the SS18 subunit of BAF chromatin remodeling complex (*SS18*), and DNA methyltransferase 3 (*DNMT3A*). Also of interest was *KIAA1009* because of its role in primary cilia function in adult cells (46) and its link to schizophrenia (47) and cognitive function (48–50). Another potentially exciting transcript was solute carrier family 18 member A2 (*SLC18A2*), a vesicular transport protein critical to monoaminergic neurotransmission (55–58). We also identified *PRKCD* (Figure 2A, C) which is particularly interesting because in rodents it marks a CeL neuron population involved in threat-processing and Pavlovian learning (Figure 2D; (32, 51, 52). CeL *PRKCD* neurons decrease their firing in response to a conditioned stimulus and interact with SST neurons to increase freezing behavior (32). Additionally, studies demonstrate that CeL *PRKCD* neurons project to the BST (39) and some of these cells play a role in negative reinforcement learning (51). Moreover, neurotrophic signaling which is associated with AT and neuropsychiatric disorders (41, 53–55), interact with PKCδ (56). In addition, *PRKCD* mRNA expression was also associated with increased freezing and decreased cooing but not

Author Manuscript Author Manuscript Author Manuscript Author Manuscript

threat-related cortisol (Figure 2E), suggesting it may be more strongly associated with the behavioral components of AT.

Characterizing PKCδ and SST neurons in the monkey CeL

While PKCδ has been extensively studied in the rodent CeL (32, 39, 51, 52, 57), little is known about its expression in the monkey. Within the CeL, many neuronal subtypes exist (58–61) and mouse studies reveal that SST neurons modulate PKCδ neurons (22, 38, 62). Because these cell types have not been well characterized in monkeys, we used stereological cell counting to map CeL PKCδ and SST neurons (Figure 3). To further understand the extent to which the mouse studies are translatable to primates, we also performed studies in the mouse CeL (Figure 3B,C). In the monkey CeL, PKCδ neurons accounted for 59% of the estimated total neurons and SST neurons accounted for 6% (Figure 3D). In the mouse CeL, PKCδ neurons constituted 43% of the estimated total neurons whereas SST neurons accounted for 20% (Figure 3D). While the proportion of PKCδ neurons did not significantly differ between species ($t=-1.06$, $p=0.34$; Figure 3E), the proportion of SST cells was notably decreased in the monkey compared to the mouse ($t=-3.6$, $p=0.02$; Figure 3E). In monkeys, 4% of neurons expressed SST and PKCδ while in mice this population was non-existent (Figure 3D).

Previous studies demonstrate that cell types are differentially distributed across the Ce's A-P extent which suggests A-P functional differences (32, 63, 64). Consistent with this, PKCδ ($t=3.1$, $p=0.01$) and SST ($t=2.6$, $p=0.02$) neurons were significantly more concentrated in the posterior mouse CeL (Figure 3F). In the monkey, SST somata were more concentrated in the posterior CeL ($t=2.7$, $p=0.012$; Figure 3F), replicating previous observations (65). However, deviating from the mouse, monkey PKCδ neurons were not differentially distributed across the A-P extent ($t=-0.39$, $p=0.7$). The interaction between A-P location and species was tested separately for PKCδ and SST neurons, and demonstrated significant interactions; PKCδ ($t=2.6$, $p=0.01$) and SST ($t=2.7$, $p=0.01$; Figure 3G).

In contrast to the small number of CeL SST neurons, and consistent with previous work, we found dense SST neuropil throughout the monkey CeL (64–67). Numerous SST varicosities were present in close apposition to the primary dendrite and soma of large CeL neurons, a number of which expressed PKCδ (Figure 3C), suggesting that in monkeys, SST input may modulate CeL PKCδ neurons. Compared to the limited distribution profile described in the mouse (32), monkey *PRKCD* expression was widely distributed across the brain (Figure S7).

A subset of CeL PKCδ neurons project to the BSTLd in the monkey

In rodents, in addition to constituting a intra-CeL microcircuit, *PRKCD* and *SST* neurons project to other parts of the extended amygdala (35, 39, 68). For example, *PRKCD* neurons project to the CeM and both *PRKCD* and *SST* neurons project to the laterodorsal BST (BSTLd; Figure 4D; (32, 35, 39, 68), suggesting that these neurons may coordinate CeL and BSTLd in mediating threat-related behaviors. Because of the lack of data in primates and the known species differences in extended amygdala organization (25), we characterized whether CeL PKCδ and SST neurons project to the BSTLd in monkeys. In six cases,

Author Manuscript Author Manuscript Author Manuscript Author Manuscript

retrograde tracers were injected into different BST subregions and in two of these cases the injections were centered in the BSTLd (J29WGA and J28WGA; Figure 4A–B). Tissue was co-labeled for the retrograde tracer, DAPI, PKCδ, and SST. Consistent with our previous observations from these monkeys (25), the cases with injections directly into the BSTLd (Figure 4A–B) demonstrated substantially more CeL retrograde labeled cells (Table 2). In these two cases, CeL retrograde-labeled cells expressing PKCδ ranged from 40–60% (Figure 4C). In contrast, few retrograde-labeled cells exclusively expressed SST or co-expressed SST and PKCδ (Figure 4C). Adding to our previous observation, SST varicosities also surrounded some CeL to BSTLd projecting neurons, a subset of which expressed PKCδ (Figure 4D). These data demonstrate that a subset of PKCδ neurons project to the BSTLd, and that SST input likely modulates this projection.

Discussion

Preclinical and clinical research has characterized the neural circuitry underlying fear and anxiety processing. In rodents, molecular studies have been performed to identify potential molecules that modulate the function of these critical neural circuits. Monkey studies are critical to translate these findings to humans and in this regard the AT model has been extremely helpful. An essential step for understanding mechanisms associated with maladaptive anxiety and in guiding new treatment development is to systematically characterize gene expression alterations in monkeys.

Here, we used a dimensional approach in AT-phenotyped monkeys, which follows the presentation of human anxiety. Our previous neuroimaging work supports the dimensionality of the AT construct at a circuit level and our search for AT-related transcripts is based on this premise. While the subsample used here did not display the highest degree of AT, the range of AT values within the subsample is representative of the larger population. In these 47 animals we performed RNA-Seq on neurons captured from the CeL, a region critically involved in gating threat-processing (20). Consistent with our previous work (45), we find that AT predicts CeL gene expression better than each of its components alone, but also that individual genes can be component-specific or component-general. This suggests that the variance in CeL gene expression can be better explained by the behavioral and endocrine AT composite than by each AT component alone, but also that specific genes or gene modules may be AT-related and still independently associated with specific AT components.

Our ontology analysis revealed overlaps between AT-associated genes and previously identified AT-related molecular pathways (41, 54). Here, a number of transcripts reflect genes that are involved in epigenetic mechanisms (69, 70); *SS18*, and *DNMT3A*), which is interesting because our earlier work suggested that AT-related Ce metabolism is predominantly affected by non-heritable factors (4). The current findings provide a molecular pathway by which epigenetic mechanisms may influence Ce function, which is particularly relevant to psychiatric disorders that are precipitated by stress (4, 71).

We also identified *KIAA1009* and *SLC18A2* as AT-related. *KIAA1009* codes for a protein located at the base of primary cilia (46) and interestingly, primary cilia alterations are

Author Manuscript Author Manuscript Author Manuscript Author Manuscript

implicated in reduced adult neurogenesis (49), poor novel object learning (48), and schizophrenia (72)(47). In addition, *SLC18A2*, which codes for VMAT2, is critical for monoaminergic neurotransmission and has been proposed as a possible drug target for some neuropsychiatric disorders (55–58). Taken together, these data support further investigation of these gene in amygdala function and psychopathology. Previously, we found an association between the truncated isoform of *NTRK3* and AT (54). However, the relatively low amount of RNA acquired with LCM precluded us from confidently examining the relations of AT and isoforms of *NTRK3*.

It is particularly exciting that CeL *PRKCD* mRNA expression was associated with AT as numerous rodent studies demonstrate that CeL *PRKCD* neurons are part of a microcircuit that modulates freezing behavior (22, 32, 38, 52, 73). Our systematic immunohistochemical characterization revealed that 59% of primate CeL neurons express PKCδ. This raises the possibility that the relation between *PRKCD* mRNA and AT could be accounted for by differences in the number of PKCδ neurons rather than differences in the expression level of PKCδ within the same number of PKCδ neurons. Unfortunately, because the tissue was fresh frozen for RNA-Seq, immunohistochemical staining could not be performed in the tissue from these animals.

Cross-species studies demonstrate that the CeL sends major projections to the BSTLd (23, 25, 33, 35, 39). We assessed the extent to which monkey CeL PKCδ neurons project to the BSTLd. Using retrograde tracers introduced into the BSTLd, we found that CeL PKCδ neurons constituted approximately half of the identified CeL to BSTLd projecting neurons. These data demonstrate that PKCδ neurons originating in the CeL project to the BSTLd. Our previous studies demonstrated that the Ce and BST are part of the neural circuit underlying AT (4) and the current data suggests a plausible pathway by which the CeL interacts with the BSTLd to coordinate AT-relevant responses. It is important to consider that approximately half of the retrograde-labeled neurons did not express PKCδ, suggesting that other CeL neuronal populations could be involved in mediating AT (33, 74, 75). We note that while *macaca mulatta* was used in the RNA-Seq experiment, *macaca fascicularis* were used in the tract-tracing experiments, and although the species are highly similar this is a potential limitation.

Rodent studies point to the importance of CeL PKCδ cells in threat-responding but do not address the role of the actual PKCδ protein. While the function of the PKCδ protein in threat-processing is unknown, PKCδ is involved in the PLC/PIP2/DAG pathway, a secondary messenger system shared by neurotrophic (76), chemokine, and membrane steroid signaling (77–79). Future studies manipulating CeL PKCδ expression will help discern the potential therapeutic value of targeting PKCδ.

CeL *PRKCD* neurons interact with other neuronal populations, including *SST* neurons (22, 32, 38). While *SST* mRNA was not associated with AT, because of its potential modulatory role, we also systematically characterized CeL SST neurons. In the monkey, SST neurons constituted a smaller population than in the mouse, however both species demonstrated dense CeL SST neuropil (58, 64, 67). We further examined monkey CeL SST varicosities and found that they have close appositions to the somata and primary dendrites of some CeL

Author Manuscript Author Manuscript Author Manuscript Author Manuscript

to BSTLd projecting neurons, including *PRKCD* neurons. The origin of the SST innervation in the monkey CeL is unknown. However, SST is expressed in GABAergic neuronal subtypes and a limited number of GABAergic regions send input to the CeL, including the BST, the sublenticular extended amygdala, and the amygdala intercalated cell masses (23, 25, 35, 80, 81). Additionally, local CeL SST neurons may also be the source of the dense SST neuropil (22, 38, 66, 82). Future studies focused on understanding the origins of CeL SST input and the effects of SST release on CeL PKCδ neurons will further our understanding of primate AT-relevant microcircuits.

This transcriptome-wide study in monkey CeL neurons provides a molecular basis for understanding alterations related to the early-life risk to develop psychopathology. This is the first study to characterize gene expression in monkey CeL neurons and to implicate CeL PKCδ neurons as components of a microcircuit relevant to primate anxiety and AT. To provide a deeper understanding of primate CeL, we systematically characterized PKCδ neurons and found potentially relevant species differences. We demonstrate that a subset of CeL PKCδ neurons project to the BSTLd and may be modulated by SST. These findings present evidence supporting a primate extended amygdala microcircuit relevant to understanding human anxiety and point to specific molecules within this circuit that could serve as potential treatment targets for anxiety disorders.

Supplementary Material

Refer to Web version on PubMed Central for supplementary material.

Acknowledgements

This work was supported by funding awarded to NHK from the NIMH (R01MH081884 and R01MH046729), and R01MH063291 awarded to JF, and RK from the NIMH (5T32MH018931), grants to the Wisconsin National Primate Center Research Center (P51-OD011106 and P51-RR000167), and the California National Primate Research Center (P51OD011107). Confocal microscopy was performed at the University of Wisconsin-Madison Biochemistry Optical Core, which was established with support from the University of Wisconsin-Madison Department of Biochemistry Endowment. We thank the Neuroscience Training Program at UW-Madison, the personnel of the Harlow Center for Biological Psychology, the HealthEmotions Research Institute, the Waisman Laboratory for Brain Imaging and Behavior, the Wisconsin National Primate Research Center, the Wisconsin Institutes for Medical Research, S. Shelton and H. Van Valkenberg. We thank L. Kordyban, A. Meier, J. Schnabel, A. Elhers for help with LCM, M. Kenwood for assistance with collating and analyzing the population behavioral data, K. Peelman for help with the mouse perfusions. A preprint of this manuscript can be found at https://t.co/B5jF6VvE9v.

References

1. Stein MB, Jang KL, Livesley WJ (1999): Heritability of anxiety sensitivity: a twin study. Am J Psychiatry. 156:246–251. [PubMed: 9989561]
2. Sawyers C, Ollendick T, Brotman MA, Pine DS, Leibenluft E, Carney DM, et al. (2019): The genetic and environmental structure of fear and anxiety in juvenile twins. American journal of medical genetics Part B, Neuropsychiatric genetics : the official publication of the International Society of Psychiatric Genetics. 180:204–212.
3. Eley TC, Bolton D, O'Connor TG, Perrin S, Smith P, Plomin R (2003): A twin study of anxiety-related behaviours in pre-school children. J Child Psychol Psychiatry. 44:945–960. [PubMed: 14531577]

Author Manuscript Author Manuscript Author Manuscript Author Manuscript

4. Fox AS, Oler JA, Shackman AJ, Shelton SE, Raveendran M, McKay DR, et al. (2015): Intergenerational neural mediators of early-life anxious temperament. Proc Natl Acad Sci U S A. 112:9118–9122. [PubMed: 26150480]
5. Fox AS, Shelton SE, Oakes TR, Davidson RJ, Kalin NH (2008): Trait-like brain activity during adolescence predicts anxious temperament in primates. PLoS ONE. 3:e2570. [PubMed: 18596957]
6. Biederman J, Hirshfeld-Becker DR, Rosenbaum JF, Herot C, Friedman D, Snidman N, et al. (2001): Further evidence of association between behavioral inhibition and social anxiety in children. Am J Psychiatry. 158:1673–1679. [PubMed: 11579001]
7. Davidson RJ, Rickman M (1999): Behavioral inhibition and the emotional circuitry of the brain: Stability and plasticity during the early childhood years In: Schmidt LA, Schulkin J, editors. Extreme fear, shyness, and social phobia: Origins, biological mechanisms, and clinical outcomes. NY: Oxford University Press, pp 67–87.
8. Hirshfeld DR, Rosenbaum JF, Biederman J, Bolduc EA, Faraone SV, Snidman N, et al. (1992): Stable behavioral inhibition and its association with anxiety disorder. J Am Acad Child Adolesc Psychiatry. 31:103–111. [PubMed: 1537760]
9. Kagan J, Reznick JS, Snidman N (1987): The physiology and psychology of behavioral inhibition in children. Child Dev 58:1459–1473. [PubMed: 3691195]
10. Essex MJ, Klein MH, Slattery MJ, Goldsmith HH, Kalin NH (2010): Early risk factors and developmental pathways to chronic high inhibition and social anxiety disorder in adolescence. Am J Psychiatry. 167:40–46. [PubMed: 19917594]
11. Chronis-Tuscano A, Degnan KA, Pine DS, Perez-Edgar K, Henderson HA, Diaz Y, et al. (2009): Stable early maternal report of behavioral inhibition predicts lifetime social anxiety disorder in adolescence. J Am Acad Child Adolesc Psychiatry. 48:928–935. [PubMed: 19625982]
12. Fox NA, Henderson HA, Marshall PJ, Nichols KE, Ghera MM (2005): Behavioral inhibition: linking biology and behavior within a developmental framework. Annual review of psychology. 56:235–262.
13. Fox AS, Kalin NH (2014): A translational neuroscience approach to understanding the development of social anxiety disorder and its pathophysiology. Am J Psychiatry. 171:1162–1173. [PubMed: 25157566]
14. Kalin NH, Shelton SE (2003): Nonhuman Primate Models to Study Anxiety, Emotion Regulation, and Psychopathology. Annals of the New York Academy of Sciences. 1008:189–200. [PubMed: 14998885]
15. Oler JA, Fox AS, Shelton SE, Rogers J, Dyer TD, Davidson RJ, et al. (2010): Amygdalar and hippocampal substrates of anxious temperament differ in their heritability. Nature. 466:864–868. [PubMed: 20703306]
16. Hettema JM, Neale MC, Kendler KS (2001): A review and meta-analysis of the genetic epidemiology of anxiety disorders. Am J Psychiatry. 158:1568–1578. [PubMed: 11578982]
17. Janak PH, Tye KM (2015): From circuits to behaviour in the amygdala. Nature. 517:284–292. [PubMed: 25592533]
18. Fox AS, Oler JA, Tromp do PM, Fudge JL, Kalin NH (2015): Extending the amygdala in theories of threat processing. Trends Neurosci 38:319–329. [PubMed: 25851307]
19. Alheid GF, Heimer L (1988): New perspectives in basal forebrain organization of special relevance for neuropsychiatric disorders: the striatopallidal, amygdaloid, and corticopetal components of substantia innominata. Neuroscience. 27:1–39. [PubMed: 3059226]
20. Fadok JP, Markovic M, Tovote P, Luthi A (2018): New perspectives on central amygdala function. Current opinion in neurobiology. 49:141–147. [PubMed: 29522976]
21. Viviani D, Charlet A, van den Burg E, Robinet C, Hurni N, Abatis M, et al. (2011): Oxytocin selectively gates fear responses through distinct outputs from the central amygdala. Science. 333:104–107. [PubMed: 21719680]
22. Fadok JP, Krabbe S, Markovic M, Courtin J, Xu C, Massi L, et al. (2017): A competitive inhibitory circuit for selection of active and passive fear responses. Nature. 542:96–100. [PubMed: 28117439]
23. Petrovich GD, Swanson LW (1997): Projections from the lateral part of the central amygdalar nucleus to the postulated fear conditioning circuit. Brain Res 763:247–254. [PubMed: 9296566]

Author Manuscript Author Manuscript Author Manuscript Author Manuscript

24. Veening JG, Swanson LW, Sawchenko PE (1984): The organization of projections from the central nucleus of the amygdala to brainstem sites involved in central autonomic regulation: a combined retrograde transport-immunohistochemical study. Brain Res 303:337–357. [PubMed: 6204716]
25. Oler JA, Tromp DP, Fox AS, Kovner R, Davidson RJ, Alexander AL, et al. (2017): Connectivity between the central nucleus of the amygdala and the bed nucleus of the stria terminalis in the non-human primate: neuronal tract tracing and developmental neuroimaging studies. Brain Struct Funct 222:21–39. [PubMed: 26908365]
26. Dong HW, Petrovich GD, Swanson LW (2001): Topography of projections from amygdala to bed nuclei of the stria terminalis. Brain research Brain research reviews. 38:192–246. [PubMed: 11750933]
27. Kim SY, Adhikari A, Lee SY, Marshel JH, Kim CK, Mallory CS, et al. (2013): Diverging neural pathways assemble a behavioural state from separable features in anxiety. Nature. 496:219–223. [PubMed: 23515158]
28. Kalin NH, Shelton SE, Davidson RJ (2004): The role of the central nucleus of the amygdala in mediating fear and anxiety in the primate. J Neurosci 24:5506–5515. [PubMed: 15201323]
29. Kalin NH, Shelton SE, Davidson RJ, Kelley AE (2001): The primate amygdala mediates acute fear but not the behavioral and physiological components of anxious temperament. Journal of Neuroscience. 21:2067–2074. [PubMed: 11245690]
30. Amaral DG, Price JL, Pitkanen A, Carmichael ST (1992): Anatomical organization of the primate amygdaloid complex. The Amygdala: Neurobiological Aspects of Emotion, Memory, and Mental Dysfunction: Wiley-Liss, Inc., pp 1–66.
31. De Olmos JS (2004): The Amygdala In: Paxinos G, Mai JK, editors. The Human Nervous System 2ed. San Diego: Elsevier Academic Press.
32. Haubensak W, Kunwar PS, Cai H, Ciocchi S, Wall NR, Ponnusamy R, et al. (2010): Genetic dissection of an amygdala microcircuit that gates conditioned fear. Nature. 468:270–276. [PubMed: 21068836]
33. Pomrenze MB, Tovar-Diaz J, Blasio A, Maiya R, Giovanetti SM, Lei K, et al. (2019): A Corticotropin Releasing Factor Network in the Extended Amygdala for Anxiety. J Neurosci 39:1030–1043. [PubMed: 30530860]
34. Asok A, Draper A, Hoffman AF, Schulkin J, Lupica CR, Rosen JB (2018): Optogenetic silencing of a corticotropin-releasing factor pathway from the central amygdala to the bed nucleus of the stria terminalis disrupts sustained fear. Molecular psychiatry. 23:914–922. [PubMed: 28439099]
35. Ahrens S, Wu MV, Furlan A, Hwang GR, Paik R, Li H, et al. (2018): A Central Extended Amygdala Circuit That Modulates Anxiety. J Neurosci 38:5567–5583. [PubMed: 29844022]
36. Yu K, Ahrens S, Zhang X, Schiff H, Ramakrishnan C, Fenno L, et al. (2017): The central amygdala controls learning in the lateral amygdala. Nat Neurosci 20:1680–1685. [PubMed: 29184202]
37. LeDoux JE, Cicchetti P, Xagoraris A, Romanski LM (1990): The lateral amygdaloid nucleus: sensory interface of the amygdala in fear conditioning. J Neurosci 10:1062–1069. [PubMed: 2329367]
38. Li H, Penzo MA, Taniguchi H, Kopec CD, Huang ZJ, Li B (2013): Experience-dependent modification of a central amygdala fear circuit. Nat Neurosci 16:332–339. [PubMed: 23354330]
39. Ye J, Veinante P (2019): Cell-type specific parallel circuits in the bed nucleus of the stria terminalis and the central nucleus of the amygdala of the mouse. Brain Struct Funct
40. Funk CM, Peelman K, Bellesi M, Marshall W, Cirelli C, Tononi G (2017): Role of Somatostatin-Positive Cortical Interneurons in the Generation of Sleep Slow Waves. J Neurosci 37:9132–9148. [PubMed: 28821651]
41. Fox AS, Oler JA, Shelton SE, Nanda SA, Davidson RJ, Roseboom PH, et al. (2012): Central amygdala nucleus (Ce) gene expression linked to increased trait-like Ce metabolism and anxious temperament in young primates. Proc Natl Acad Sci U S A. 109:18108–18113. [PubMed: 23071305]
42. Zimin AV, Cornish AS, Maudhoo MD, Gibbs RM, Zhang X, Pandey S, et al. (2014): A new rhesus macaque assembly and annotation for next-generation sequencing analyses. Biology Direct. 9:20. [PubMed: 25319552]

Author Manuscript Author Manuscript Author Manuscript Author Manuscript

43. Love MI, Huber W, Anders S (2014): Moderated estimation of fold change and dispersion for RNA-seq data with DESeq2. Genome Biology. 15:550. [PubMed: 25516281]
44. Mi H, Muruganujan A, Ebert D, Huang X, Thomas PD (2018): PANTHER version 14: more genomes, a new PANTHER GO-slim and improvements in enrichment analysis tools. Nucleic Acids Research. 47:D419–D426.
45. Shackman AJ, Fox AS, Oler JA, Shelton SE, Davidson RJ, Kalin NH (2013): Neural mechanisms underlying heterogeneity in the presentation of anxious temperament. Proc Natl Acad Sci U S A. 110:6145–6150. [PubMed: 23538303]
46. Wang WJ, Tay HG, Soni R, Perumal GS, Goll MG, Macaluso FP, et al. (2013): CEP162 is an axoneme-recognition protein promoting ciliary transition zone assembly at the cilia base. Nature cell biology. 15:591–601. [PubMed: 23644468]
47. Munoz-Estrada J, Lora-Castellanos A, Meza I, Alarcon Elizalde S, Benitez-King G (2018): Primary cilia formation is diminished in schizophrenia and bipolar disorder: A possible marker for these psychiatric diseases. Schizophrenia research. 195:412–420. [PubMed: 28927861]
48. Wang Z, Phan T, Storm DR (2011): The type 3 adenylyl cyclase is required for novel object learning and extinction of contextual memory: role of cAMP signaling in primary cilia. J Neurosci 31:5557–5561. [PubMed: 21490195]
49. Amador-Arjona A, Elliott J, Miller A, Ginbey A, Pazour GJ, Enikolopov G, et al. (2011): Primary cilia regulate proliferation of amplifying progenitors in adult hippocampus: implications for learning and memory. J Neurosci 31:9933–9944. [PubMed: 21734285]
50. Berbari NF, Malarkey EB, Yazdi SM, McNair AD, Kippe JM, Croyle MJ, et al. (2014): Hippocampal and cortical primary cilia are required for aversive memory in mice. PLoS ONE. 9:e106576. [PubMed: 25184295]
51. Cui Y, Lv G, Jin S, Peng J, Yuan J, He X, et al. (2017): A Central Amygdala-Substantia Innominata Neural Circuitry Encodes Aversive Reinforcement Signals. Cell reports. 21:1770–1782. [PubMed: 29141212]
52. Yu K, Garcia da Silva P, Albeanu DF, Li B (2016): Central Amygdala Somatostatin Neurons Gate Passive and Active Defensive Behaviors. J Neurosci 36:6488–6496. [PubMed: 27307236]
53. Turner CA, Clinton SM, Thompson RC, Watson SJ Jr., Akil H (2011): Fibroblast growth factor-2 (FGF2) augmentation early in life alters hippocampal development and rescues the anxiety phenotype in vulnerable animals. Proc Natl Acad Sci U S A. 108:8021–8025. [PubMed: 21518861]
54. Fox AS, Souaiaia T, Oler JA, Kovner R, Kim JMH, Nguyen J, et al. (2019): Dorsal Amygdala Neurotrophin-3 Decreases Anxious Temperament in Primates. Biol Psychiatry.
55. Duman RS, Li N (2012): A neurotrophic hypothesis of depression: role of synaptogenesis in the actions of NMDA receptor antagonists. Philosophical transactions of the Royal Society of London Series B, Biological sciences. 367:2475–2484. [PubMed: 22826346]
56. Newton AC (2010): Protein kinase C: poised to signal. Am J Physiol Endocrinol Metab. 298:E395–402. [PubMed: 19934406]
57. Amano T, Amir A, Goswami S, Pare D (2012): Morphology, PKCdelta expression, and synaptic responsiveness of different types of rat central lateral amygdala neurons. J Neurophysiol 108:3196–3205. [PubMed: 22972957]
58. Cassel MD, Gray TS (1989): Morphology of Peptide Immunoreactive neurons in the rat central nucleus of the amygdala. Journal of Comparative Neurology.320–333. [PubMed: 2468696]
59. Price JL, Russchen FT, Amaral DG (1987): The limbic region. II. The amygdaloid complex In: Hokfelt BT, Swanson LW, editors. Handbook of Chemical Neuroanatomy. Amsterdam: Elsevier, pp 279–381.
60. Roberts GW, Woodhams PL, Polak JM, Crow TJ (1982): Distribution of neuropeptides in the limbic system of the rat: the amygdaloid complex. Neuroscience. 7:99–131. [PubMed: 6176906]
61. McCullough KM, Morrison FG, Hartmann J, Carlezon WA Jr., Ressler KJ (2018): Quantified Coexpression Analysis of Central Amygdala Subpopulations. eNeuro 5.
62. Kim J, Zhang X, Muralidhar S, LeBlanc SA, Tonegawa S (2017): Basolateral to Central Amygdala Neural Circuits for Appetitive Behaviors. Neuron 93:1464–1479.e1465. [PubMed: 28334609]

Author Manuscript Author Manuscript Author Manuscript Author Manuscript

63. Han W, Tellez LA, Rangel MJ Jr., Motta SC, Zhang X, Perez IO, et al. (2017): Integrated Control of Predatory Hunting by the Central Nucleus of the Amygdala. Cell. 168:311–324.e318. [PubMed: 28086095]
64. Amaral DG, Avendano C, Benoit R (1989): Distribution of somatostatin-like immunoreactivity in the monkey amygdala. J Comp Neurol 284:294–313. [PubMed: 2568998]
65. Kovner R, Fox AS, French DA, Roseboom PH, Oler JA, Fudge JL, et al. (2019): Somatostatin Gene and Protein Expression in the Non-human Primate Central Extended Amygdala. Neuroscience. 400:157–168. [PubMed: 30610938]
66. Cassell MD, Gray TS, Kiss JZ (1986): Neuronal architecture in the rat central nucleus of the amygdala: a cytological, hodological, and immunocytochemical study. J Comp Neurol 246:478–499. [PubMed: 2422231]
67. Martin LJ, Powers RE, Dellovade TL, Price DL (1991): The bed nucleus-amygdala continuum in human and monkey. J Comp Neurol 309:445–485. [PubMed: 1918444]
68. Cai H, Haubensak W, Anthony TE, Anderson DJ (2014): Central amygdala PKC-delta(+) neurons mediate the influence of multiple anorexigenic signals. Nat Neurosci 17:1240–1248. [PubMed: 25064852]
69. Lubieniecka JM, de Bruijn DRH, Su L, van Dijk AHA, Subramanian S, van de Rijn M, et al. (2008): Histone Deacetylase Inhibitors Reverse SS18-SSX–Mediated Polycomb Silencing of the Tumor Suppressor Early Growth Response 1 in Synovial Sarcoma. Cancer Research. 68:4303–4310. [PubMed: 18519690]
70. Tang L, Nogales E, Ciferri C (2010): Structure and Function of SWI/SNF Chromatin Remodeling Complexes and Mechanistic Implications for Transcription. Progress in biophysics and molecular biology. 102:122–128. [PubMed: 20493208]
71. Elbau IG, Cruceanu C, Binder EB (2019): Genetics of Resilience: Gene-by-Environment Interaction Studies as a Tool to Dissect Mechanisms of Resilience. Biol Psychiatry. 86:433–442. [PubMed: 31202489]
72. Pruski M, Lang B (2019): Primary Cilia-An Underexplored Topic in Major Mental Illness. Frontiers in psychiatry. 10:104. [PubMed: 30886591]
73. Ciocchi S, Herry C, Grenier F, Wolff SB, Letzkus JJ, Vlachos I, et al. (2010): Encoding of conditioned fear in central amygdala inhibitory circuits. Nature. 468:277–282. [PubMed: 21068837]
74. Gray TS, Magnuson DJ (1992): Peptide immunoreactive neurons in the amygdala and the bed nucleus of the stria terminalis project to the midbrain central gray in the rat. Peptides 13:451–460. [PubMed: 1381826]
75. Moga MM, Gray TS (1985): Evidence for corticotropin-releasing factor, neurotensin, and somatostatin in the neural pathway from the central nucleus of the amygdala to the parabrachial nucleus. J Comp Neurol 241:275–284. [PubMed: 2868027]
76. Rankin SL, Guy CS, Rahimtula M, Mearow KM (2008): Neurotrophin-induced upregulation of p75NTR via a protein kinase C-delta-dependent mechanism. Brain Res 1217:10–24. [PubMed: 18511024]
77. Kanehisa M, Goto S (2000): KEGG: kyoto encyclopedia of genes and genomes. Nucleic Acids Res 28:27–30. [PubMed: 10592173]
78. Kanehisa M, Sato Y (2019): KEGG Mapper for inferring cellular functions from protein sequences. Protein Sci
79. Greene MW, Morrice N, Garofalo RS, Roth RA (2004): Modulation of human insulin receptor substrate-1 tyrosine phosphorylation by protein kinase Cdelta. The Biochemical journal. 378:105–116. [PubMed: 14583092]
80. Pare D, Smith Y (1993): The intercalated cell masses project to the central and medial nuclei of the amygdala in cats. Neuroscience. 57:1077–1090. [PubMed: 8309544]
81. Gungor NZ, Yamamoto R, Pare D (2015): Optogenetic study of the projections from the bed nucleus of the stria terminalis to the central amygdala. J Neurophysiol 114:2903–2911. [PubMed: 26400259]
82. Gray TS, Cassell MD, Williams TH (1982): Synaptology of three peptidergic neuron types in the central nucleus of the rat amygdala. Peptides 3:273–281. [PubMed: 6126863]

Author Manuscript Author Manuscript Author Manuscript Author Manuscript

83. Paxinos G, Huang X, Petrides M, Toga AW (2009): The Rhesus Monkey Brain: Stereotaxic Coordinates. Elsevier.

84. Schindelin J, Arganda-Carreras I, Frise E, Kaynig V, Longair M, Pietzsch T, et al. (2012): Fiji: an open-source platform for biological-image analysis. Nature Methods. 9:676. [PubMed: 22743772]

Author Manuscript Author Manuscript Author Manuscript Author Manuscript

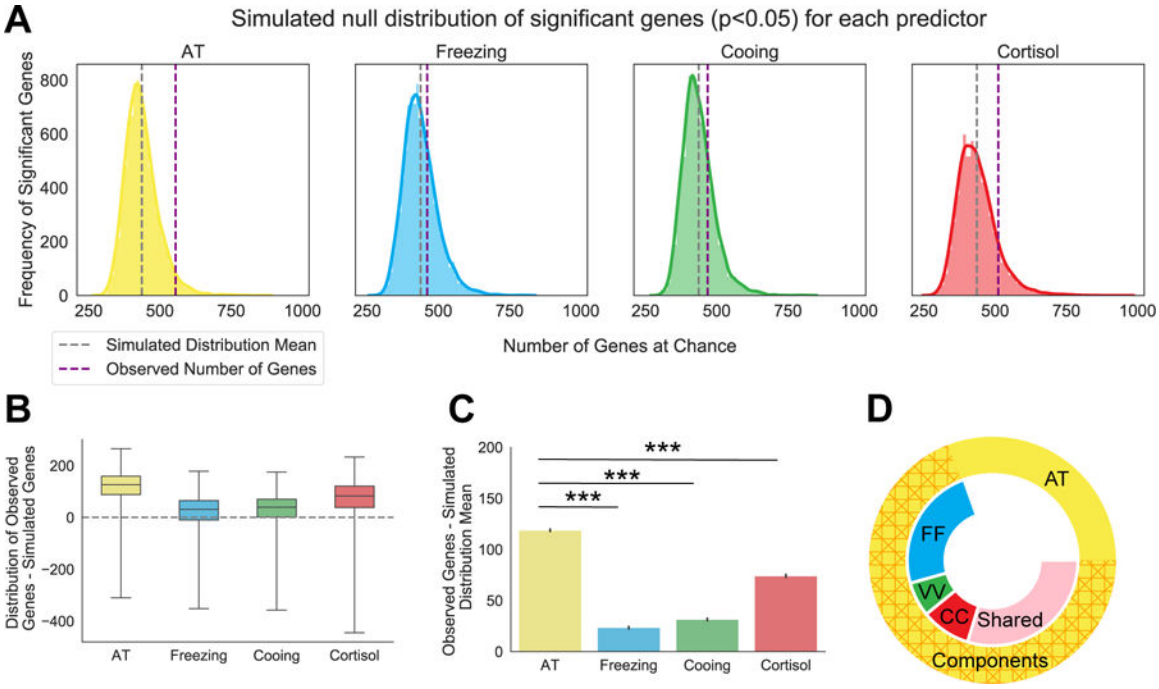

Figure 1. AT predicts a significant number of genes above chance and outperforms each of the AT components.

(A) Simulated null distribution (as described in the methods section RNA Sequencing Analysis and Statistics) for each predictor of interest at a nominal p-value of $p<0.05$. Purple dotted lines indicate the observed number of genes associated with each predictor's real values. Grey dotted lines indicate the mean number of genes of the simulated distribution. Solid colored outline of the distribution represents the density of significant genes as determined by a kernel density estimation. (B) Boxplots for each predictor depicting the distribution and mean of the differences between the real observation and each simulated value. Empirical p-values were calculated for each predictor, AT: p=0.04, freezing: p=0.3, cooing: p=0.24, cortisol: p=0.12 (C) Barplot demonstrating that AT predicts significantly more genes above the simulated distribution mean than those predicted by each of the AT components alone: freezing ($t=113.5$, $p<0.001$), cooing ($t=106.9$, $p<0.001$), or cortisol ($t=496$, $p<0.001$). Error bars are displayed as SEM. P-values are Šidák corrected for multiple comparisons. AT component values were transformed and residualized as described in the Methods: Anxious Temperament phenotyping (D) Donut plot depicting the number of overlapping genes between individual AT components and AT. Outside circle represents all 555 AT-related genes ($p<0.05$) and is separated into the 393 genes that overlap with AT components (hashed orange) and the 172 genes that are unique to AT (yellow). Inner circle represents genes that are related to AT and is broken up by genes that are also unique to one AT component (FF: freezing in blue, VV: cooing in green, CC: cortisol in red) or that are shared by at least two components (shared in pink).

Author Manuscript Author Manuscript Author Manuscript Author Manuscript

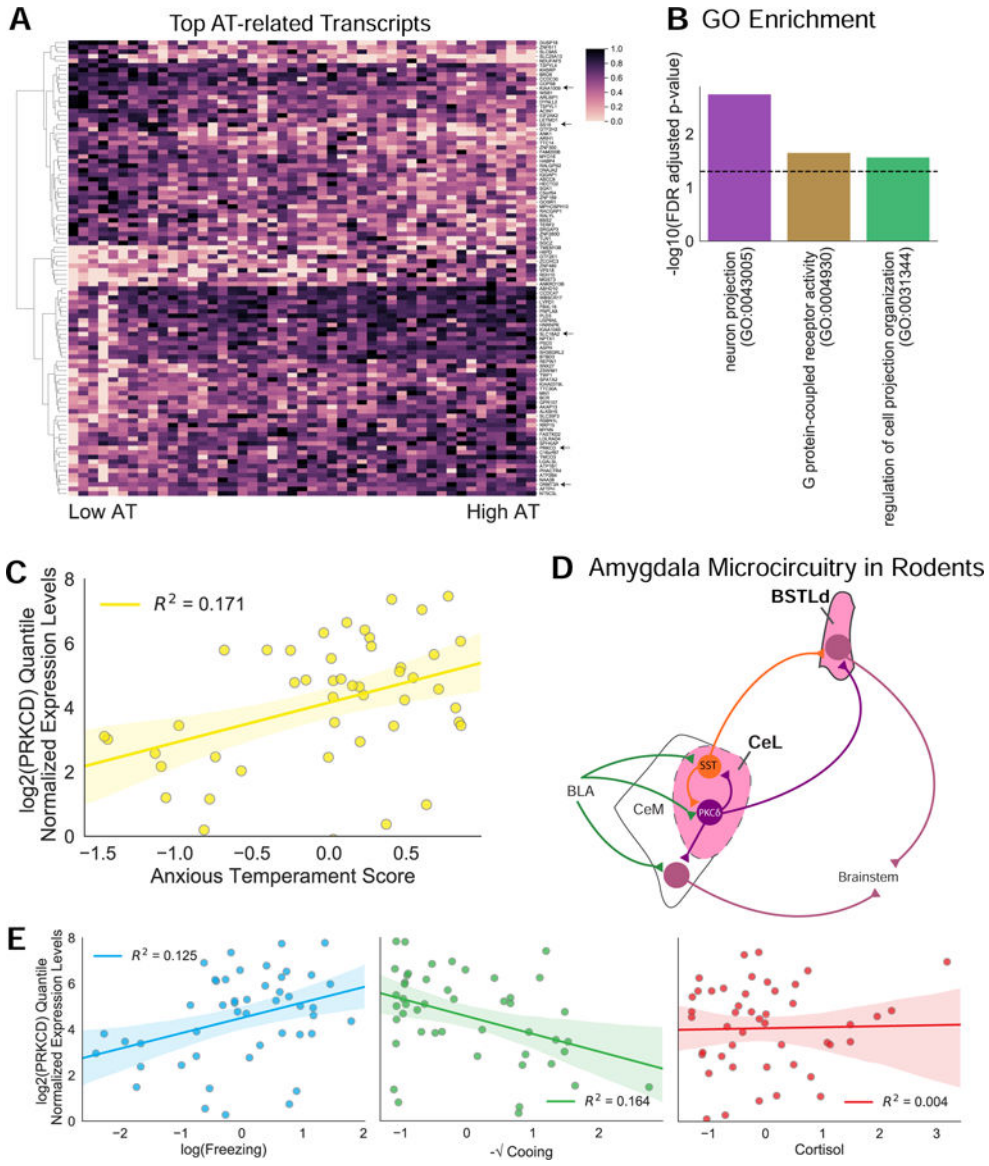

Figure 2. RNA-Seq of LCM CeL neurons revealed AT-related genes.

(A) Heatmap displaying the top 100 AT-related genes from the intersection of the OLS and DEseq2 analyses ($p<0.05$). Gene expression data are presented as quantile normalized min-max scaled values. Arrows point to genes that are discussed in the text. (B) Subset of GO enrichment groups for cellular component (purple), molecular function (yellow) and biological process (green) that overlap between approaches. The FDR-corrected p-value is depicted by the black dashed line. FDR values reflect those from the OLS ontology. All statistics can be found in Table S2. (C) Correlation between *PRKCD* mRNA expression levels and AT (R^2=0.171). Shaded areas represent the SEM. (D) Simplified diagram of the microcircuit within the rodent amygdala and extended amygdala. PKCδ expressing neurons are labeled in purple. SST expressing neurons are labeled in orange. Previous work demonstrates that SST and PKCδ expressing neurons both receive information from the basolateral amygdala complex (BLA) and contribute to an inhibitory microcircuit within the

Author Manuscript Author Manuscript Author Manuscript Author Manuscript

CeL (32, 38, 39). Both cell types also project to the laterodorsal BST (BSTLd) while PKCδ expressing neurons but not SST neurons project to the CeM (32, 38, 39). (E) Correlations between *PRKCD* mRNA expression levels and the individual components of AT (freezing; R^2=0.125, cooing; R^2=0.164, cortisol; R^2=0.004; OLS regression). Freezing, cooing, and cortisol values were standardized, transformed, and residualized as described in the methods. *PRKCD* mRNA expression levels are presented as quantile normalized log2 transformed values residualized for age at ToD and CeL neuron accuracy.

Author Manuscript Author Manuscript Author Manuscript Author Manuscript

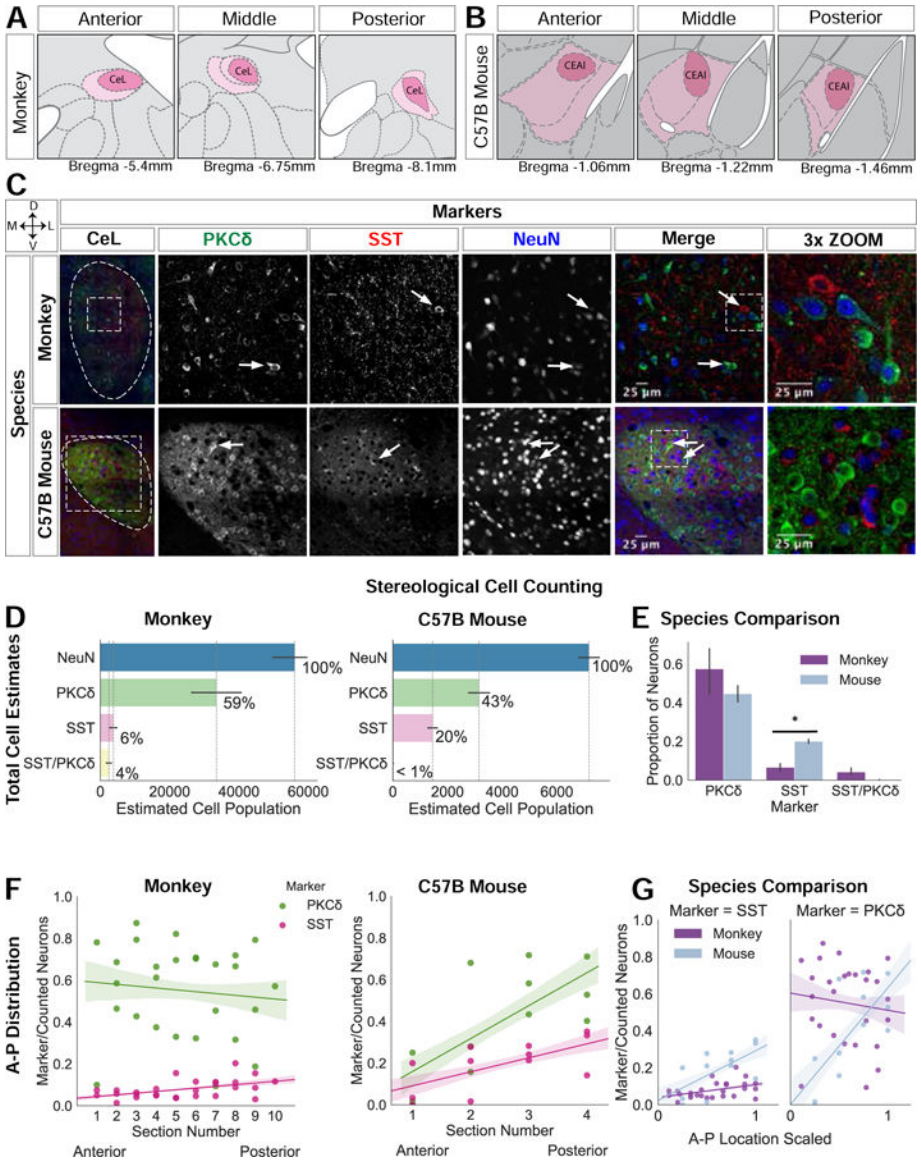

Figure 3. PKCδ expressing neurons in the monkey compared to the mouse CeL.

(A) CeL atlas slices depicting the A-P extent in the rhesus monkey (83); (B) and in the mouse (Allen Brain Atlas). (C) Representative confocal images of the CeL in both species; white arrows point to PKCδ and SST neurons. Images were adjusted using the Fiji despeckle filter (84) for removing salt and pepper noise. (D) Stereological cell estimates for monkey (n=3) and mouse (n=3). (E) Species comparison of PKCδ, SST, and PKCδ/SST estimates are presented as a proportion of the total number of neurons (PKCδ: t=−1.06, p=0.34, SST: t=3.6, p=0.02; t-test), error bars are SEM. (F) A-P distribution of PKCδ and SST expressing neurons in monkey and mouse (monkey: PKCδ p=0.7, t=−0.39 and SST p=0.012, t=2.7, mouse: PKCδ p=0.01, t=3.1, SST p=0.02, t=2.6; OLS regression). (G) Species comparison of the A-P distribution of each cell type (A-P location X species interaction for PKCδ (t=2.6, p=0.01) and A-P location X species interaction for SST (t=2.7, p=0.01); OLS

Author Manuscript Author Manuscript Author Manuscript Author Manuscript

regression). To compare A-P distribution between species, A-P location was min-max scaled with 0 indicating more anterior slices and 1 indicating more posterior slices.

Author Manuscript Author Manuscript Author Manuscript Author Manuscript

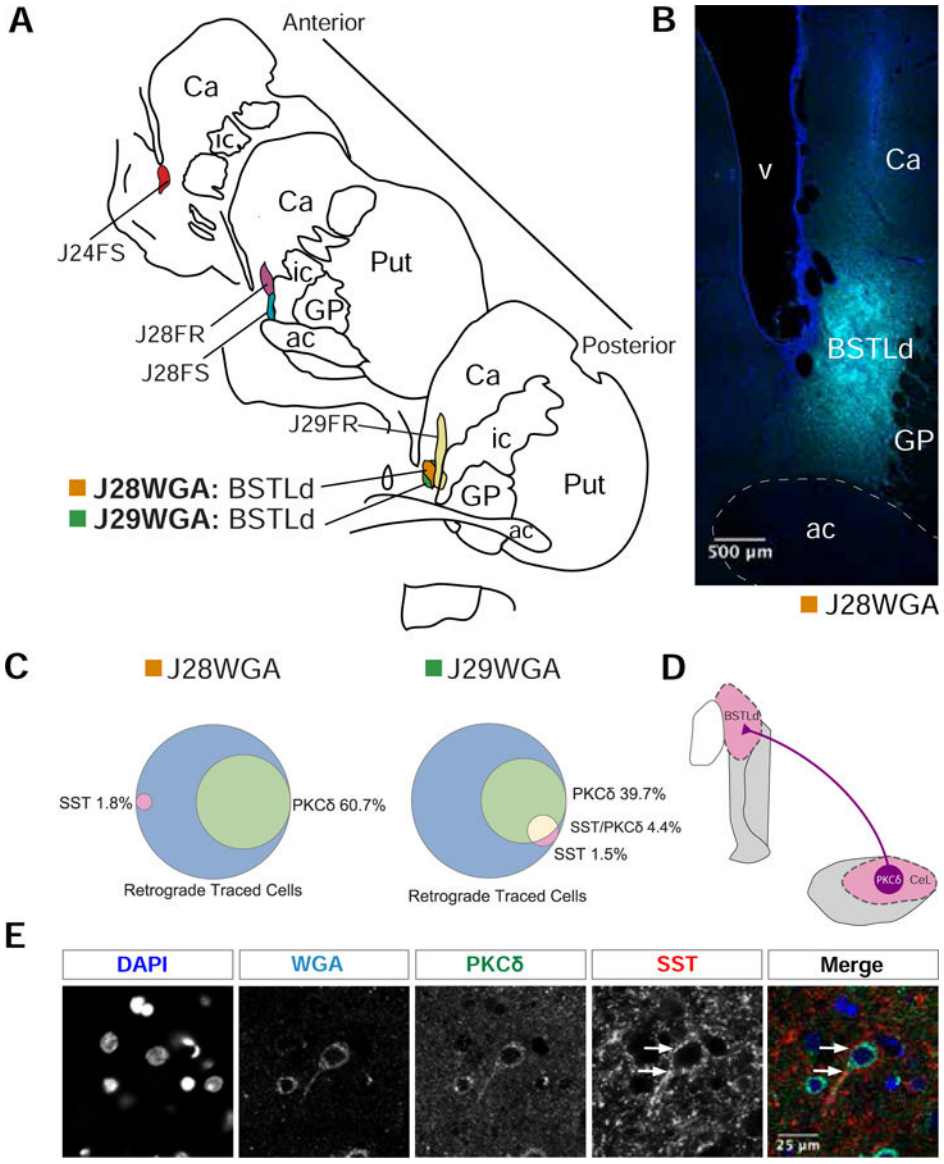

Figure 4. A subset of PKCδ expressing neurons project to the BSTLd in the monkey.

(A) Hand drawn slices depicting the localization of retrograde tracer into different regions of the BST in monkey. Two replicates, J29WGA and J28WGA, are localized to the same part of the BSTLd. (B) Representative confocal image of the BSTLd injection site. DAPI staining is in blue. WGA-tracer staining is in cyan. (C) A Venn diagram for each BSTLd replicate, J29WGA and J28WGA, illustrating the percent overlap between the WGA-tracer and PKCδ, SST, or both. (D) Simplified diagram of our results demonstrating that CeL PKCδ expressing neurons project to the BSTLd in nonhuman primates. (E) Representative confocal image of a BSTLd-projecting neuron that expresses PKCδ. This image was adjusted using the Fiji despeckle filter (84) for removing salt and pepper noise. White arrows point to the immense SST innervation received along this neuron's primary dendrite and soma.

Author Manuscript Author Manuscript Author Manuscript Author Manuscript

Table 1.

Verified gene hits that pass multiple comparison correction across two different statistical methods. Functions of interest were chosen based on ontologies that contain these genes. AT relation indicates the direction of the gene expression correlation with AT.

Gene	Functions of interest	AT relation
chr18: SS18	Nuclear receptor transcription coactivator activity (GO:0030374) Positive regulation of transcription, DNA-templated (GO:0045893)	−
chr02a: DNMT3A	DNA binding (GO:0003677) Chromatin binding (GO:0003682)	+
chr05: ZNF300	Sequence-specific DNA binding (GO:0043565)	−
chr03: PRKCD	Intracellular signal transduction (GO:0035556) Protein kinase C activity (GO:0004697)	+
chr06: SH3BGRL2	SH3 domain binding (GO:0017124)	+
chr15: BCR	Protein binding (GO:0005515)	+
chr16: FBXL16	Ubiquitin-protein transferase activity (GO:0004842)	+
chr02a: AFTPH	Clathrin binding (GO:0030276) Intracellular transport (GO:0046907)	+
chr17: DYNLL2	Dynein light intermediate chain binding (GO:0051959)	−
chr10: SLC18A2	Monoamine transmembrane transporter activity (GO:0008504)	+
chr06: KIAA1009	Protein binding (GO:0005515)	−
chr01: MGST3	Glutathione transferase activity (GO:0004364)	+
chr09: KIAA1045	Regulation of synaptic transmission, GABAergic (GO:0032228)	+
chr16:C16orf87	Protein binding (GO:0005515)	+

Author Manuscript

Author Manuscript

Author Manuscript

Author Manuscript

Table 2.

Number and percentage of retrograde tracer-labeled cells expressing markers of interest for each case of retrograde injection.

Case ID	Retrograde tracer type	# Retrograde-labeled Cells	Retrograde-labeled Cells Expressing PKCδ		Retrograde-labeled Cells Expressing SST		Retrograde-labeled Cells Expressing PKCδ and SST	
			#	%	#	%	#	%
J24FS	FS	8	1	12.5	1	12.5	0	0
J28FS	FS	23	8	34.8	2	8.7	0	0
J28FR	FR	8	6	75.0	0	0	0	0
J29FR	FR	2	1	50.0	0	0	0	0
J28WGA	WGA	56	34	60.7	2	1.8	0	0
J29WGA	WGA	136	54	39.7	2	1.5	6	4.4

Author Manuscript Author Manuscript Author Manuscript Author Manuscript

KEY RESOURCES TABLE

Resource Type	Specific Reagent or Resource	Source or Reference	Identifiers	Additional Information
Add additional rows as needed for each resource type	Include species and sex when applicable.	Include name of manufacturer, company, repository, individual, or research lab. Include PMID or DOI for references; use “this paper” if new.	Include catalog numbers, stock numbers, database IDs or accession numbers, and/or RRIDs. RRIDs are highly encouraged; search for RRIDs at https://scicrunch.org/resources.	Include any additional information or notes if necessary.
Antibody	PKCd anti-rabbit	Cell Signaling Technologies	cat# 2058, lot# 4	0.032 mg/ml, 150000 dalton, 1:200 dilution
Antibody	PKCd anti-mouse	BD Biosciences	cat# 610397, lot# 3280966	0.25 mg/ml, 150000 dalton, 1:500 dilution
Antibody	PKCd anti-rabbit	Thermo Fisher	cat# PA5-17552, lot# SK2476171c, UF2791897A	0.032 mg/ml, 150000 dalton, 1:200 dilution
Antibody	SST anti-goat	Santa Cruz	cat# sc-7819, lot# G1813	0.1 mg/ml, 1:2000 dilution
Antibody	SST anti-mouse	Santa Cruz	cat# sc-74556, lot# L3109	0.2 mg/ml, 1:2000 dilution
Antibody	NeuN anti-mouse	Thermo Fisher	cat# MAB377, lot# 2829834	0.5 mg/ml, 1:2000 dilution
Antibody	Rhodamine anti-mouse	Rockland antibodies and assays	cat# 200-301-246, lot# 39545	1mg/ml, 1:1000 dilution
Antibody	Fluorescin anti-goat	Rockland antibodies and assays	cat# 600-101-096, lot# 32951	1mg/ml, 1:1000 dilution
Antibody	Wheat-germ agglutinin anti-goat	VectorLabs	cat# A52024, lot# ZE0312	1mg/ml, 1:1000 dilution
Antibody	AlexaFluor 488 donkey anti-goat	ThermoFisher	cat# A11055, lot# 1827671	2 mg/ml, 1:250 dilution
Antibody	AlexaFluor 568 donkey anti-goat	ThermoFisher	cat# A11057, lot# 1711491	2 mg/ml, 1:250 dilution
Antibody	AlexaFluor 647 donkey anti-goat	ThermoFisher	cat# A21447, lot# 2045332	2 mg/ml, 1:250 dilution
Antibody	AlexaFluor 568 donkey anti-rabbit	ThermoFisher	cat# A10042, lot# 1964370	2 mg/ml, 1:250 dilution
Antibody	AlexaFluor 488 donkey anti-rabbit	ThermoFisher	cat# A21206, lot# 1910751, 1874771	2 mg/ml, 1:250 dilution
Antibody	AlexaFluor 568 donkey anti-mouse	ThermoFisher	cat# A10037, lot# 1827879	2 mg/ml, 1:250 dilution
Antibody	AlexaFluor 647 donkey anti-mouse	ThermoFisher	cat# A31571, lot# 1839633	2 mg/ml, 1:250 dilution
Antibody	DAPI	ThermoFisher	cat# D1306	10 mg/ml, 1:10,000 dilution
Peptide	PKCd purified peptide	ABCam	cat# Ab27714-1, lot# 359579	0.02 mg/ml, 78,000 dalton
Biological Sample	Postmortum rhesus monkey tissue	University of Wisconsin, Kalin laboratory		
Organism/Strain	Mouse: C57BL/6J, male	The Jackson Laboratory	RRID:IMSR_JAX:000664	
Organism/Strain	Mouse: B6;129X1-Prkcdtm1Msg/J, male	The Jackson Laboratory	RRID:IMSR_JAX:028055	

Author Manuscript Author Manuscript Author Manuscript Author Manuscript

Resource Type	Specific Reagent or Resource	Source or Reference	Identifiers	Additional Information
Chemical Compound or Drug	Ketamine	Midwest Veterinary Supply	cat# 193.40551.3, 193.85100.3	
Chemical Compound or Drug	Donkey Serum	Jackson ImmunoResearch Laboratories, West Grove, PA	cat# 017-000-121	
Commercial Assay Or Kit	DPC Coat-a-count radioimmunoassay	Siemens, Los Angeles, CA		
Commercial Assay Or Kit	NuGen RNA-Seq V2 kit	NuGen, San Carlos, CA	cat# 7102-32	
Commercial Assay Or Kit	NuGEN Ovation Rapid library kit	NuGen, San Carlos, CA	cat# 0319, 0320	
Commercial Assay Or Kit	ImmunoPact DAB	Vector Laboratories	cat# SK-4105	
Commercial Assay Or Kit	Qiagen RNeasy Plus micro kit	Qiagen, Hilden, Germany	cat# 74034	
Software; Algorithm	DESeq2	DOI: 10.18129/B9.bioc.DESeq2	RRID:SCR_015687	
Software; Algorithm	StereoInvestigator 2018.1.1	MBF Bioscience, Williston, VT USA		
Software; Algorithm	SAGE	https://github.com/tadesouaiaia/sage		